NUMERICAL SIMULATION OF CONVECTIVE HEAT TRANSFER COEFFICIENT IN CHANNEL WITH CORRUGATED WALLS

by

Serge KEWOU, Marcel EDOUN*, Olivier Mba TAWETSING, and Alexis KUITCHE

Laboratory of Energetic and Applied Thermal Process,
Department of Energetic, Electrical and Automatic Engineering,
ENSAI, University of Ngaoundere, Yaounde, Cameroon

Original scientific paper
https://doi.org/10.2298/TSCI150615061K

The present work is a contribution to study of convective heat transfer coefficient inside a rectangular channel with corrugated walls. Triangular, square, and rectangular shaped configurations were studied for a range of geometric parameters during simulation. The Navier-Stokes equations were numerically solved using the finite volume method through the EasyCFD_G package code in its V.4.1.0 version. With prescribed temperatures and velocities, the model predicts the behavior of the air-flow inside the device. The temperature and velocity distributions are first predicted. From these distributions, the convective heat transfer coefficients along the surface of the objects placed inside the system are determined. Also, from the pressure distribution, the pressure drops along the channel are predicted. The results show that the triangular corrugated-shaped configuration with h = 5 cm and α = β = 60° enable to obtain the best value of convective heat transfer coefficient on the surface of the objects which is 2.70 W/m^2°C resulting in a pressure drop of 0.11 Pa, while for parallel-plate channel configuration this same coefficient is 1.12 W/m^2°C. The energy balance enabled to conclude that the energy gain by convection air/objects is superior to the air pump energy to overcome the pressure drop.

Key words: *corrugated walls, convective transfer coefficient, pressure drop, numerical simulation*

Introduction

In order to reduce the post-harvests losses which are estimated at approximately 40% in southern countries [1], several solutions have been proposed including drying. Drying commonly describes the process of thermally removing volatile substances (moisture) to yield a solid product. It is a mechanism involving the complex phenomena of simultaneous heat and mass transfers between the air and products. Convective transfer coefficients are one of the most critical parameters required for the analysis and simulation of the drying process [2]. Convective heat transfer coefficient, h_c, quantifies the heat crossing a product per unit time, surface and temperature degree, it is an important parameter in drying rate simulation since the temperature difference between the air and products varies with this coefficient [3]. Therefore, it is necessary to analyze the influence of this coefficient on the drying of the products.

* Corresponding author, e-mail: edounmarcel@yahoo.fr

Many experimental and theoretical studies for determination of the convective heat transfer coefficient have been reported in the literature [4-12]. These studies show that the convective heat transfer coefficient strongly depends on a number of external parameters including temperature and velocity of the air. Furthermore, drying is an energy intensive operation that easily accounts for up to 15% of all industrial energy usages, often with relatively low thermal efficiency in the range of 25-50%. In this regard, it would be interesting to improve the convective heat transfer coefficient for better thermal drying efficiency.

Numerous publications have been devoted to the study of creative ways of increasing the heat transfer rate in compact heat exchangers [13-16], as well as in the flat plate air solar collector [17-20]. The symmetric corrugated or wavy-walled channel is one of several devices utilized for enhancing the heat transfer efficiency. They promote higher heat transfer coefficients by disturbing or altering the existing flow behavior (except for extended surfaces) which also leads to increase in the pressure drop [13]. It is therefore worthwhile to study the performance of these types of devices on the heat transfer between the air and objects placed inside the duct.

The aim of this work is to examine the influence of the insertion of corrugated walls in a rectangular channel on the heat transfer coefficient between the air and objects placed inside the channel. This is to numerically study the effect of the corrugated walls adding different geometric parameters on the thermodynamic behavior of the air, and to predict the temperature and velocity distributions inside the channel and around objects.

Material and methods

Problem configuration

Figure 1 shows the problem domain, with the corresponding boundary conditions, for the evaluation of velocity and temperature distributions of air around the objects. The objects are kept inside a rectangular channel 0.6 m × 0.2 m and exposed to the flow of hot air through the channel. The objects are placed centrally at the middle of the channel so that it gets maximum exposure to the air-flow.

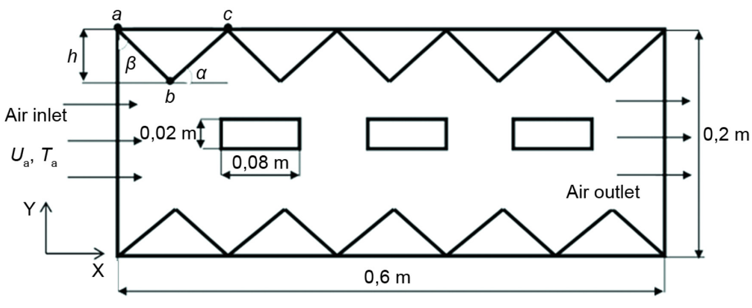

Figure 1. Problem geometry

To evaluate convective heat transfer coefficient between the air and objects, we inserted corrugated walls arranged on both longitudinal sides of the channel. Triangular, square and rectangular shaped configurations were studied for a range of geometric parameters grouped according to the configurations in tab. 1, where *ba, bc*, and *h* [cm], represent the geometric dimensions according to the corrugated walls shape studied, *α* and *β* represent the angles of inclination.

Governing equations

The partial differential eqs. (1)-(6) governing the forced convection motion of a fluid in a 2-D geometry are the mass continuity, momentum, and energy conservation equations. In the simplified case, thermal and physical properties are assumed to be constant (*i. e.*, the variation of fluid properties with temperature has been neglected). Considering the flow incompressible, for a 2-D problem, the most general form of the Navier-Stokes equations is given [20]:

Table 1. Geometric parameters of corrugated walls

Configurations	Geometrical characteristics				
	ab	*bc*	*h*	*α* [°]	*β* [°]
W0			0		
W1	6	6	3	30	60
W2	4.24	4.24	3	45	45
W3	3.46	3.46	3	60	30
W4	10	10	5	30	60
W5	7.07	7.07	5	45	45
W6	5.77	5.77	5	60	30
C1	3	3	3	90	00
C2	5	5	5	90	00
R1	5	5	3	90	00
R2	3	3	5	90	00

Continuity equation

$$\frac{\partial(\rho u)}{\partial x}+\frac{\partial(\rho v)}{\partial y} \quad (1)$$

Momentum conservation equations

– horizontal component

$$\frac{\partial(\rho u^2)}{\partial x}+\frac{\partial(\rho uv)}{\partial y}=-\frac{\partial P}{\partial x}+\frac{\partial}{\partial x}\left[\Gamma\left(2\frac{\partial u}{\partial x}-\frac{2}{3}\mathrm{div}\vec{\mathrm{V}}\right)\right]+\frac{\partial}{\partial y}\left[\Gamma\left(\frac{\partial u}{\partial y}-\frac{\partial v}{\partial x}\right)\right] \quad (2)$$

– vertical component

$$\frac{\partial(\rho v^2)}{\partial y}+\frac{\partial(\rho uv)}{\partial x}=-\frac{\partial P}{\partial y}+\frac{\partial}{\partial y}\left[\Gamma\left(2\frac{\partial v}{\partial x}-\frac{2}{3}\mathrm{div}\vec{\mathrm{V}}\right)\right]+\frac{\partial}{\partial x}\left[\Gamma\left(\frac{\partial u}{\partial y}-\frac{\partial v}{\partial x}\right)\right]+I \quad (3)$$

In the previous equations, P [Nm^{-2}] represents pressure, and I – the buoyancy forces. The diffusion coefficient is, in this case, given by:

$$\Gamma=\mu+\mu_{\mathrm{t}} \quad (4)$$

where μ [Nsm^{-2}] is the dynamic viscosity, and μ_{t} – the turbulent viscosity.

Energy conservation equation

In this case, the dependent variable is the enthalpy $Ø = C_pT$:

$$\frac{\partial(\rho C_p uT)}{\partial x}+\frac{\partial(\rho C_p vT)}{\partial y}=\frac{\partial}{\partial x}\left(\Gamma\frac{\partial T}{\partial x}\right)+\frac{\partial}{\partial y}\left(\Gamma\frac{\partial T}{\partial y}\right)+S_T \quad (5)$$

Term S_T, represents the heat generation rate per unit volume [Wm^{-3}]. The diffusion coefficient is, for the case of a fluid domain:

$$\Gamma=\frac{\mu}{\mathrm{Pr}}+\frac{\mu_{\mathrm{t}}}{\mathrm{Pr_t}} \quad (6)$$

Turbulence modeling

The properties of a turbulent flow (velocity, pressure, *etc.*) are not constant in time, instead, they present oscillations about an average value. The numerical calculation of the instantaneous value is not amenable with present day techniques and resources, due to the high temporal and spatial frequencies that characterize these flows [20]. We are, thus, left with the calculation of the average values only. These can be described through the Reynolds decomposition:

$$\hat{\O} = \O + \O' \tag{7}$$

where $\hat{\O}$ is the instantaneous value, $\O$ – the average value, and $\O'$ – the difference between the two (fluctuation). When the Reynolds decomposition is applied to the transport equations and the equations are the averaged, some extra terms appear, due to the following property. Illustrated for the third term of eq. (2):

$$\rho uv = \rho \overline{uv} + \rho \overline{u'v'} \tag{8}$$

The last term in the previous equation has the dimensions of a stress and thus, can be expressed as the product of a viscosity (turbulent viscosity) by an average velocity gradient, as in the case of the laminar stresses (this hypothesis was proposed by Boussinesq). The computation of the turbulent viscosity is made recurring to a turbulence model. EasyCFD_G implements the *k-ε* and the shear stress transport (STT) models. For this study, we used the STT model.

The standard formulation of this turbulence model is described by [20-23]. The turbulent viscosity is given by:

$$\mu_\mathrm{t} = C_\mu \frac{\rho k^2}{\varepsilon} \tag{9}$$

where k [m^{-2}s^{-2}] is the turbulence kinetic energy. The turbulence kinetic energy, k, as well as its dissipation rate, ε [m^{-2}s^{-3}] are computed with the following transport equations:

$$\frac{\partial(\rho uk)}{\partial x} + \frac{\partial(\rho vk)}{\partial y} = \frac{\partial}{\partial x}\left[\left(\mu + \frac{\mu_\mathrm{t}}{\sigma_\mathrm{k}}\right)\frac{\partial k}{\partial x}\right] + \frac{\partial}{\partial y}\left[\left(\mu + \frac{\mu_\mathrm{t}}{\sigma_\mathrm{k}}\right)\frac{\partial k}{\partial y}\right] + P_\mathrm{k} - \rho\varepsilon + G_\mathrm{T} \tag{10}$$

$$\frac{\partial(\rho u\varepsilon)}{\partial x} + \frac{\partial(\rho v\varepsilon)}{\partial y} = \frac{\partial}{\partial x}\left[\left(\mu + \frac{\mu_\mathrm{t}}{\sigma_\varepsilon}\right)\frac{\partial \varepsilon}{\partial x}\right] + \frac{\partial}{\partial y}\left[\left(\mu + \frac{\mu_\mathrm{t}}{\sigma_\varepsilon}\right)\frac{\partial \varepsilon}{\partial y}\right] + \frac{\varepsilon}{k}C_1 P_\mathrm{k} - C_2\rho\varepsilon + C_3 G_\mathrm{T} \tag{11}$$

The term P_k represents the production rate of k as the results of the velocity gradients:

$$P_\mathrm{k} = \mu_\mathrm{t}\left[2\left(\frac{\partial u}{\partial x}\right)^2 + 2\left(\frac{\partial v}{\partial y}\right)^2 + \left(\frac{\partial u}{\partial y} + \frac{\partial v}{\partial x}\right)^2\right] \tag{12}$$

while the term G_T accounts for the production or destruction of k and ε due to the thermal gradients:

$$G_\mathrm{T} = -\beta \mathrm{g} \frac{\mu_\mathrm{t}}{\mathrm{Pr}_\mathrm{t}} \frac{\partial T}{\partial y} \tag{13}$$

The remaining model constants are [20-23]:

$C_\mu = 0{,}09$, $\sigma_\mathrm{k} = 1{,}0$, $\sigma_\varepsilon = 1{,}3$, $C_1 = 1{,}44$, $C_2 = 1{,}92$, and $C_3 = 1{,}44$

Numerical method

The EasyCFD_G package code in its V.4.1.0 version based on the finite volume method is used to transform and solve the previous equations. The discretization scheme used is hybrid for the convective terms in the momentum and energy equations, and the SIMPLEC algorithm for pressure-velocity coupling. The boundary conditions assume no-slip conditions for velocity, constant temperature on the surface of the objects.

From the velocity fields obtained, the convective heat transfer coefficient, h_c, along the surface of the objects can be determined using the following correlation of the air flowing to a plane surface [24]:

$$h_c = B V_{\mathrm{a}}^{0.8} \tag{14}$$

where B is the constant, and V_{a} – the inlet air velocity of the channel.

We will calculate the power required for pumping air and heat power supplied to the objects from eqs. (15) and (16), respectively:

$$P_u = Q_{\mathrm{v}} \Delta P \tag{15}$$

$$Ø_{\mathrm{conv}} = h_c S (T_{\mathrm{a}} - T_{\mathrm{p}}) \tag{16}$$

where Q_{v} is the volumetric flow rate, ΔP – the pressure loss in the section, and S – the area of the object.

Comparison of these powers will enable us to determine whether we can achieve an energy gain with the use of corrugated-walled.

Results and discussion

Simulations are carried out for an inlet velocity of 0.5 m/s. The objective of performing the CFD simulation is to calculate the heat transfer coefficient on the surface of the objects placed in the channel. The heat transfer coefficient is independent of the imposed temperature at the inlet, wall of the channel and the boundaries of the objects as long as the properties are assumed to be constant. In the simulation, an inlet temperature T_{a} = 45 °C and wall temperature $T = T_{\mathrm{a}}$ is assumed. The boundaries of the objects are also set at T_{p} = 20 °C.

Evaluation of convective heat transfer coefficient

Configurations W0, W1, W2, and W3

The temperature distribution in the channel and around the objects for configurations W0, W1, W2, and W3 was presented in fig. 2. Almost identical change in temperature is observed in the channel and around the objects for each configuration. The temperature is constant and equal to the set temperature at the inlet of the channel and diverged way along the surface of the objects. It reduces the contact of the air with the objects. This is due to the temperature difference between the air and objects. The average temperature on the surface of the objects is 37.85, 38.29, 38.20, and 38.22 °C for the configurations W0 – fig. 2(a), W1 – fig. 2(b), W2 – fig. 2(c), and W3 – fig. 2(d), respectively. Thus we can see that the presence of triangular corrugated-shaped lightly influences the temperature distribution in the channel.

Figure 3 presents the velocity distribution in the channel and around the objects for configurations W0, W1, W2, and W3. In fig. 3(a) is observed that the velocity at the entrance of the channel is high, due to the existence of unsteady vortex shedding to the first level

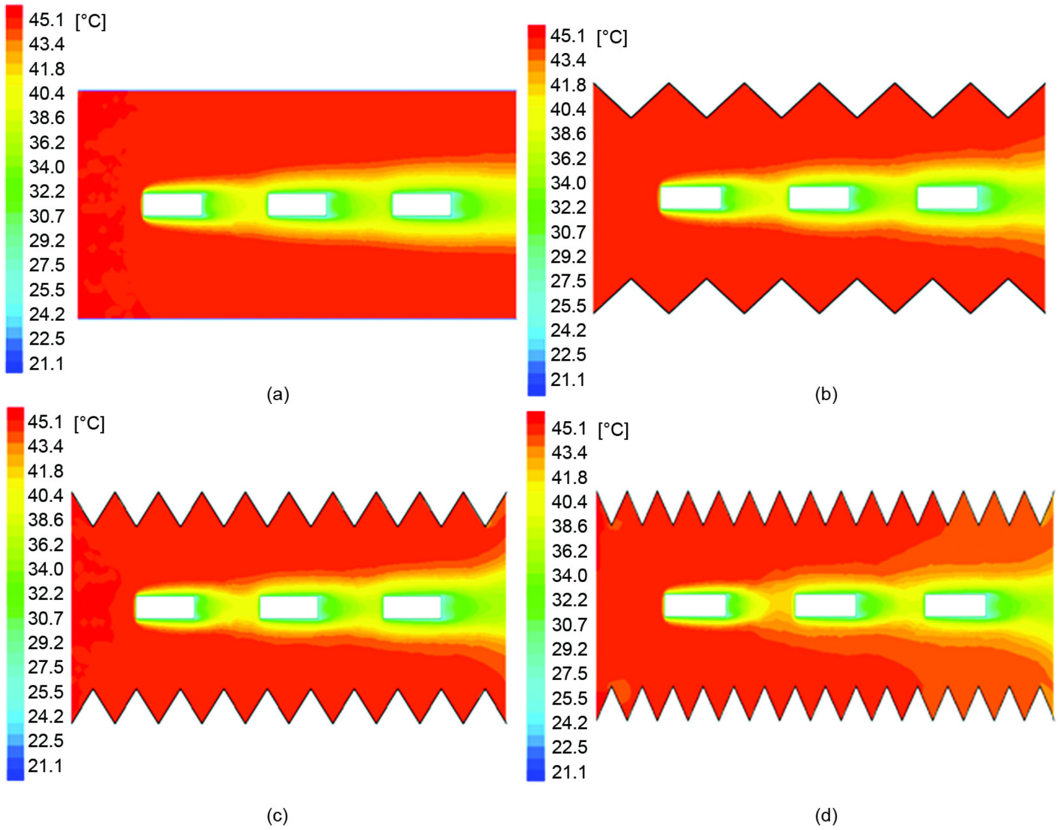

Figure 2. Temperature distribution at different configurations; W0 (a), W1 (b), W2 (c), and W3 (d)
(*for color image see journal web-site*)

object it generates a take-off velocity which will form the boundary-layers at the surface of the objects. This is explained by the fact that the object behave she eras a barrier to the flow of air. For figs. 3(b), (c), and (d) the takeoff velocity is generated here by the corrugated walls and thus observed high air velocities around objects. They vary from 0.61 to 0.91 m/s, 0.70 to 1.04 m/s, and from 0.69 to 1.03 m/s for configurations W1, W2, and W3, respectively. The average values of the velocity at the surface of objects are 0.84, 0.90, and 0.90 m/s for configurations W1, W2, and W3, respectively, and 0.49 m/s for the configuration W0. Thus we find that the presence of triangular corrugated-shaped in the channel increases the velocity of the air around the objects, and this increase is a function of the tilt angle of the corrugated walls.

Figure 4 presents the h_c profiles along the surface of the objects for configurations W0, W1, W2, and W3. This coefficient varies lightly along the surface of the objects and moves identically for all configurations. The average value of h_c is 1.12 W/m^2°C for configuration W0. This value considerably increases when introducing corrugated walls in the channel. It is 1.74, 1.84, and 1.85 W/m^2°C for configurations W1, W2, and W3, respectively. Thus, as h_c strongly depends on the velocity, an increase in this rate necessarily increases the convective heat transfer coefficient.

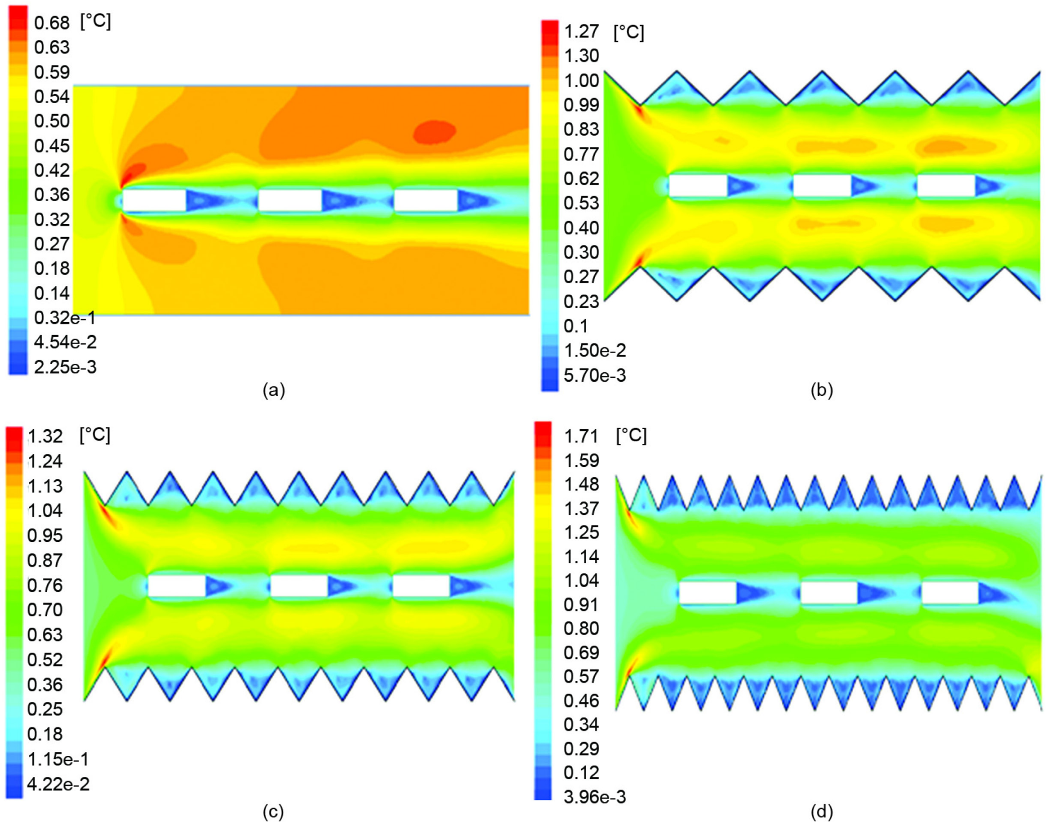

Figure 3. Velocity distribution at different configurations; W0 (a), W1 (b), W2 (c), and W3 (d)
(*for color image see journal web-site*)

Configurations W0, W4, W5, and W6

The temperature distribution in the channel and around the objects for configurations W0, W4, W5, and W6 was presented in fig. 5. As in previous configurations, the temperature is changing almost identically in the channel for each case. The average values of temperature on the surface of objects are 38.65, 38.45, and 38.69 °C for configurations W4, W5, and W6, respectively. Thus we see that the increase in the height of the triangular corrugated-shaped lightly affects the temperature distribution in the channel.

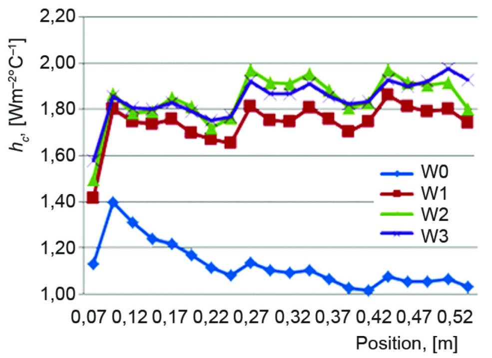

Figure 4. Convective heat transfer coefficients profiles at different configurations; W0, W1, W2, and W3

Figure 6 presents the velocity distribution in the channel and around the objects for configurations W0, W4, W5, and W6. It is observed that the velocity is substantially increased and it is constant along the surface of the objects for configurations W4, W5, and W6.

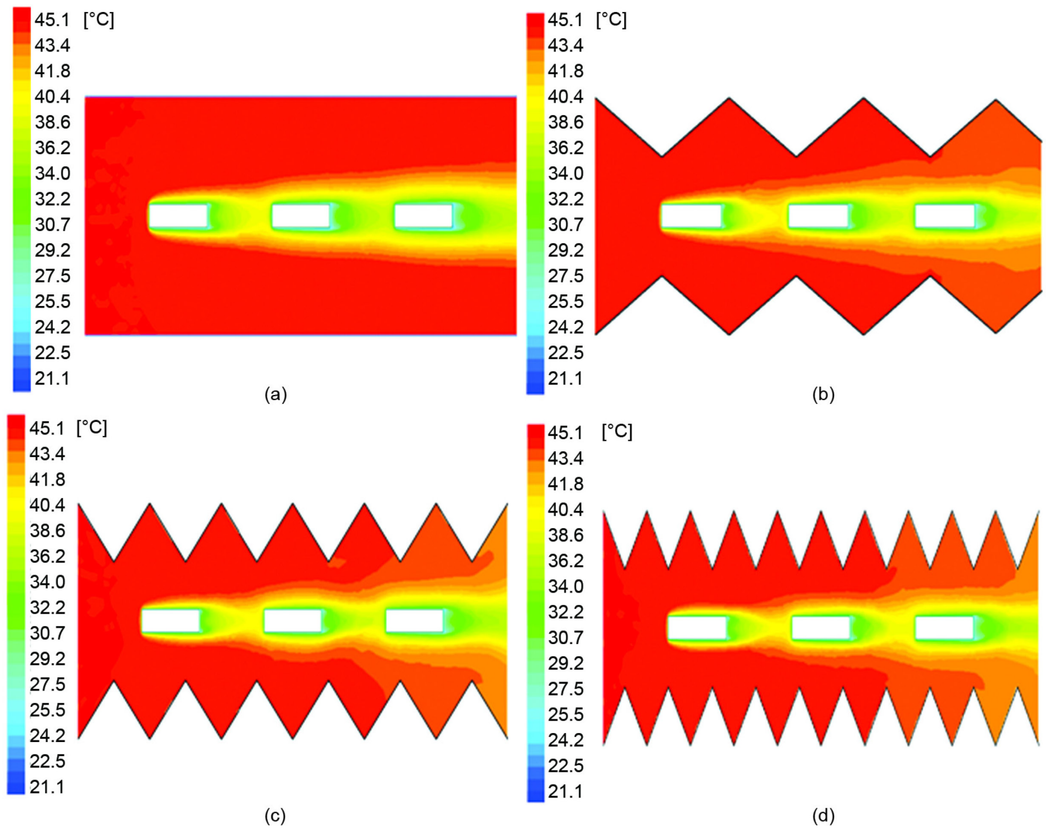

Figure 5. Temperature distribution at different configurations; W0 (a), W4 (b), W5 (c), and W6 (d)
(*for color image see journal web-site*)

It varies from 0.63 to 1.25 m/s, 0.66 to 1.26 m/s, and 0.69 to 1.37 m/s for configurations W4, W5, and W6, respectively. The average values of the velocity on the surface of the objects are 1.18, 1.41, and 1.46 m/s for configurations W4, W5, and W6, respectively, and 0.49 m/s for configuration W0. Thus we see that the increase of the height of the corrugated walls can greatly increase the velocity of the air around the objects, and this increase is a function of the tilt angle of the corrugated walls.

Figure 7 is the representation of the h_c profiles along the surface of the objects for configurations W0, W4, W5, and W6. Increasing the height of the triangular corrugated-shaped greatly increases the convective heat transfer coefficient. The average values of h_c are 2.29, 2.63, and 2.70 W/m^2°C for the configurations W0, W4, W5, and W6, respectively. These values are very high compared to that of the parallel-plate channel (configuration W0) that is 1.12 W/m^2°C.

It is therefore apparent that the increase in height of the triangular corrugated-shaped causes a steep rise in the convective heat transfer coefficient at the objects level.

Configurations C1, C2, R1, and R2

Figure 8 presents the temperature distribution in the channel and around the objects for configurations C1, C2, R1, and R2. The temperature distribution in the channel is the

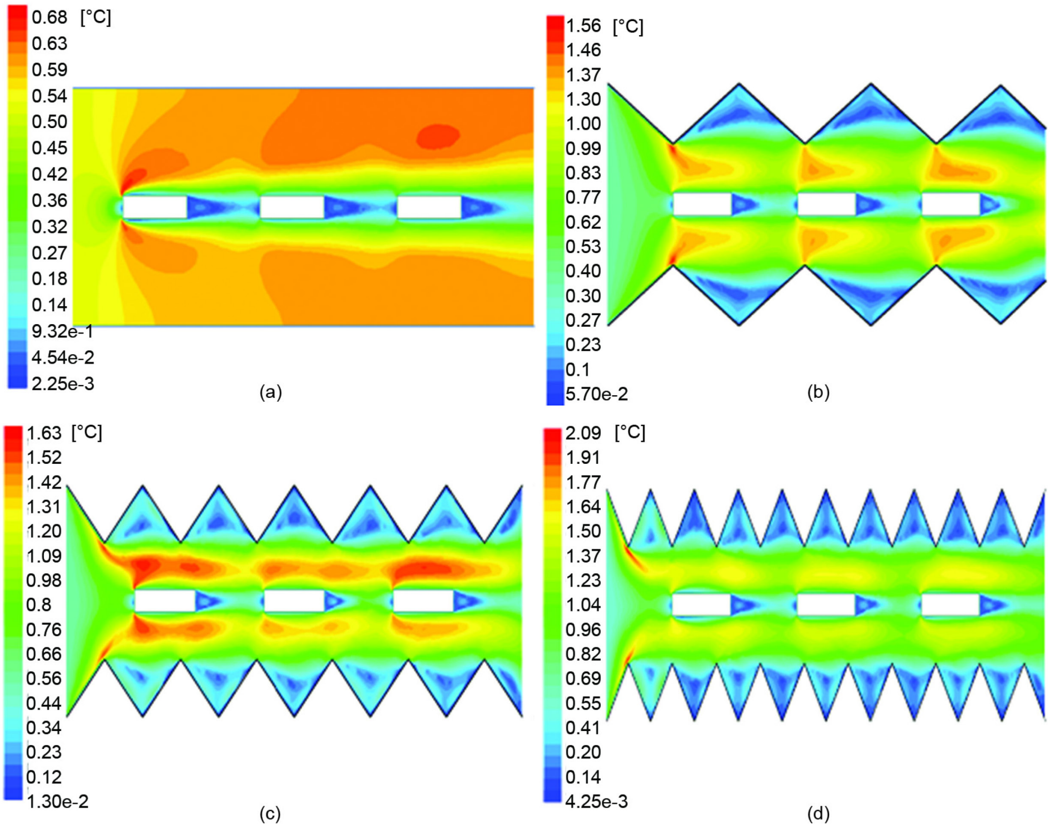

Figure 6. Velocity distribution at different configurations; W0 (a), W4 (b), W5 (c), and W6 (d)
(*for color image see journal web-site*)

same for all configurations. The temperature is constant at the entrance of the channel and diverged way along the surface of the objects. The average values of temperature along the surface of the objects are 38.34, 38.66, 38.32, and 38.69 °C for the configurations C1, C2, R1, and R2, respectively. Thus, the use of square and rectangular corrugated-shaped slightly influences the temperature distribution in the channel.

Figure 9 presents the velocity distribution for configurations C1, C2, R1, and R2. For all configurations, slightly higher velocities observed at the entrance of the channel and near-zero velocities at the corrugated walls along the canal, this is due to dead zones generated by the shape of the obstacle. On the other hand these velocities are very high along the surface of the objects. Indeed, they

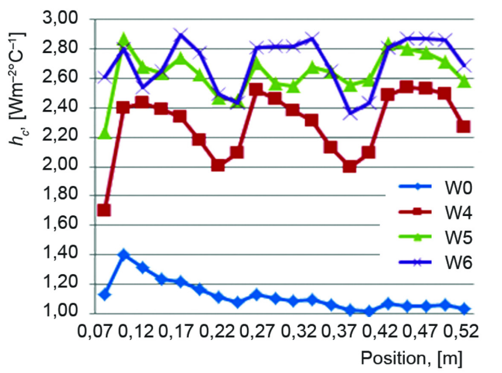

Figure 7. Convective heat transfer coefficients profiles at different configurations: W0, W4, W5, and W6

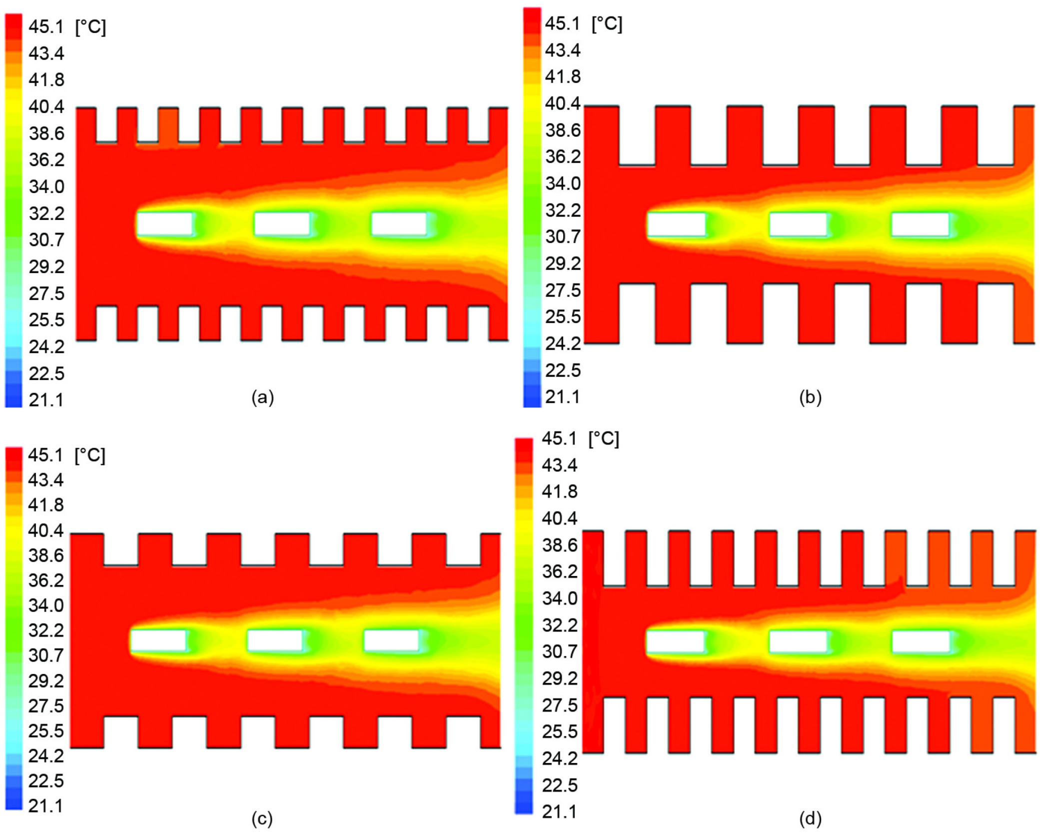

Figure 8. Temperature distribution at different configurations; C1 (a), C2 (b), R1 (c), and R2 (d)
(*for color image see journal web-site*)

vary from 0.77 to 0.98 m/s, 1.11 to 1.33 m/s, 0.61 to 0.89 m/s, and 0.60 to 1.43 m/s along the channel for the configurations C1, C2, R1, and R2, respectively. The average values of velocities on the surface of the objects are 0.82, 1.33, 0.84, and 1.39 m/s for the configurations C1, C2, R1, and R2, respectively. Thus, we find that the presence of square and rectangular corrugated-shaped can greatly increase the velocity of the air at the surface of the objects.

Figure 10 presents the h_c profiles along the surface of the objects for configurations C1, C2, R1, and R2. It shows the same trend of the convective heat transfer coefficient for both configurations C1 and R1 for C2 and R2 configurations. This is due to the almost similar disposition of these corrugated walls in the channel. However, it has very high values of h_c for all configurations with respect to the configuration W0. Thus, the average values of the heat transfer coefficient obtained on the surface of the objects are 1.71, 2.70, 1.74, and 2.61 W/m^2°C for configurations C1, C2, R1, and R2, respectively. While the average value of h_c for configuration W0 is 1.12 W/m^2°C. It is apparent that the insertion of square and rectangular corrugated-shaped in the channel also significantly increases the convective heat transfer coefficient at the surface of objects.

It appears from the analysis of these temperature ranges and air velocity that the addition of obstacles in the dynamic vein of the air has a significant effect on the convective heat transfer coefficient. However, this influence is based on the layout, shape and dimensions of the obstacle. This analysis allows us to conclude that the triangular shaped configuration W6 (h_{cW6} = 2.70 W/m^2°C), square shaped configuration C2 (h_{cC2} = 2.70 W/m^2°C) and the rectangular shaped configuration R2 (h_{cR2} = 2.61 W/m^2°C), produce the best average values of the heat transfer coefficients on the surface of objects.

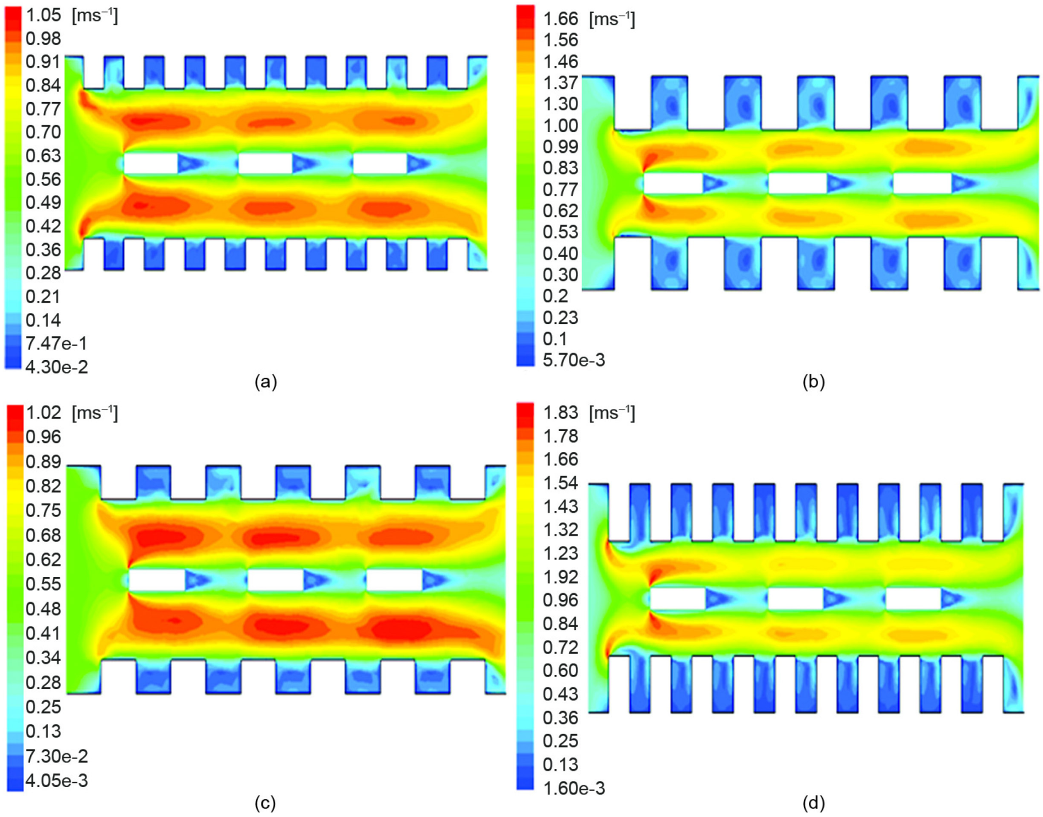

Figure 9. Velocity distribution at different configurations; C1 (a), C2 (b), R1 (c), and R2 (d) (*for color image see journal web-site*)

Evaluation of pressure drops

Since configurations W6, C2 and R2 make it possible to obtain the best average values of h_c, we will evaluate the pressure drops caused by the use of these types of corrugated walls configurations. Figure 11 is the representation of the pressure distribution for configurations W0, W6, C2, and R2. It is found that the pressure is high at the entrance of the channel but drop low along the air circuit in the channel for configuration W0. For configurations W6, C2, and R2 pressure is very high at the entrance and

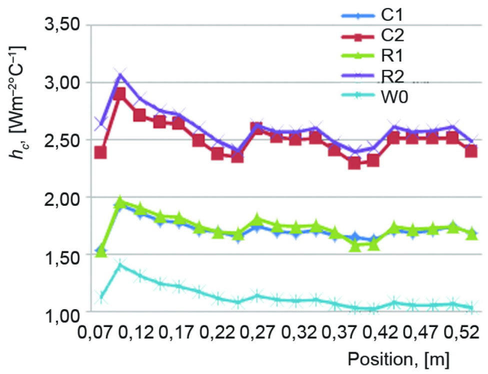

Figure 10. Convective heat transfer coefficients profiles at different configurations: C1, C2, R1, and R2

significantly drop along the channel. This drop varies with the shape of the corrugated walls. Thus, the values of the pressure between the inlet and the outlet of the channel vary from 0.24 to 0.18 Pa, 2.24 to 0.26 Pa, 3.26 to 1.67 Pa, and 4.20 to 2.62 Pa, for configurations W0, W6, C2, and R2, respectively.

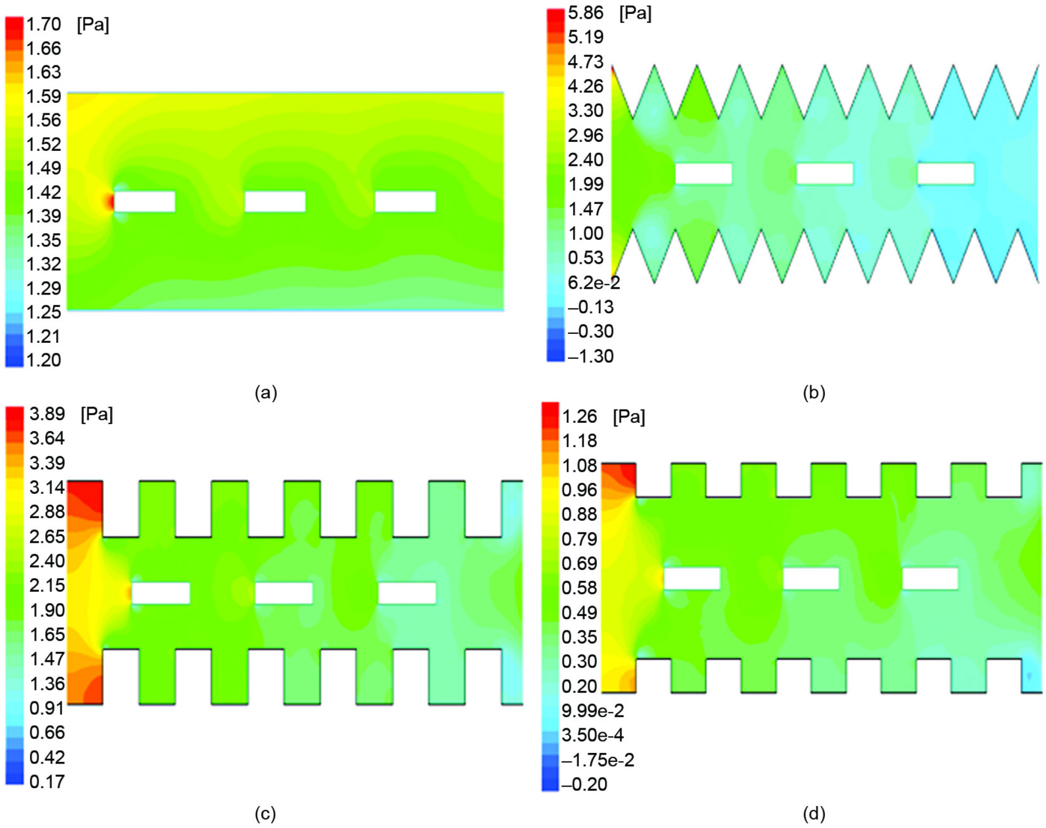

Figure 11. Pressure distribution at different configurations; W0 (a), W6 (b), C2 (b), and R2 (d)
(*for color image see journal web-site*)

Evaluation of the air pump power and the heat power

This is about determining the powers for the configuration W6. A comparison of thermal powers between configurations W0 and W6 is recorded in tab. 2.

Table 2. Thermal energy

Configurations	T_a [°C]	T_p [°C]	h_c [Wm^{-2}°C^{-1}]	$Ø_{conv}$ [W]	ΔP [Pa]	P_u [W]
W6	45	20	2.70	0.108	0.11	$6.6\cdot10^{-3}$
W0	45	20	1.12	0.0448	0	0
Difference			1.58	0.0632	0.11	$6.6\cdot10^{-3}$

It appears that the power required overcoming the pressure drop for the configuration W6 is 6.6×10^{-3} W and thermal power exchanged by convection is 0.108 W. For configuration W0 this thermal power is only 0.0448 W. This leads to a gain of about 0.0566 W. Thus, we find that the configuration W6 improves the heat exchange between the air and the objects while limiting the energy consumption of the system ventilation.

Conclusion

The aim of this work is to examine the influence of the insertion of corrugated walls in a rectangular channel on the heat transfer coefficient between the air and objects placed inside the channel. The analysis of the temperature and velocity distributions for all configurations studied revealed that the addition of obstacles in the dynamic vein of the air has a significant influence on the convective heat transfer coefficient. The results obtained enabled us to highlight that the triangular corrugated-shaped configuration have a convective heat exchange coefficient greater than the square corrugated-shaped. Unfortunately, these configurations generate more important pressure drops. Despite this, the power balance exchanged by convection shows that the energy gain is greater than the energy required to overcome the pressure drops by ventilation.

Nomenclature

C_p – constant pressure specific heat, [$\mathrm{Jkg^{-1}K^{-1}}$]
h_c – heat transfer coefficient, [$\mathrm{Wm^{-2}K^{-1}}$]
h – height, [m]
I – buoyancy forces
k – turbulence kinetic energy, [$\mathrm{m^2s^{-2}}$]
$Ø_{\mathrm{conv}}$ – convection thermal power, [W]
P_u – output power, [W]
P – pressure, [$\mathrm{Nm^{-2}}$]
ΔP – pressure loss, [Pa]
Q_{v} – volumetric flow rate, [$\mathrm{m^3s^{-1}}$]
S – aera of the objet, [$\mathrm{m^2}$]
T – temperature, [°C]
u, v – velocities in x- and y-direction, [$\mathrm{ms^{-1}}$]
V – velocity, [$\mathrm{ms^{-1}}$]

Greek symbols

α, β – angle of inclination, [°]
Γ – diffusion coefficient
ε – dissipation rate, [$\mathrm{m^2s^{-3}}$]
μ – dynamic viscosity, [$\mathrm{Nsm^{-2}}$]
ρ – density, [$\mathrm{kgm^{-3}}$]

Subscripts

a – air
p – product
t – turbulent

References

[1] Edoun, M., *et al.*, Situation of Artisanal Drying Practices of Fruits and Vegetables in the Southern Cameroon (in French), *Fruits, 66* (2010), 1, pp. 1-12
[2] Ratti, C., Crapiste, G. H., Determination of Heat Transfer Coefficients during Drying of Foodstuffs, *Journal of Food Processing Engineering, 18* (1995), 1, pp. 41-53
[3] Anwar, S. I., Tiwari, G. N., Evaluation of Convective Heat Transfer Coefficient in Crop Drying under Open Sun Drying, *Energy Conversion Management, 42* (2001), 5, pp. 627-637
[4] Goyal, R. K., Tiwari, G. N., Heat and Mass Transfer Relation for Crop Drying, *Drying Technology, 16* (1998), 8, pp. 1741-1754
[5] Anwar, S. I., Tiwari, G. N., Convective Heat Transfer Coefficient of Crop in Forced Convection Drying: An Experimental Study, *Energy Conversion Management, 42* (2001), 14, pp. 1687-1698
[6] Togrul, I. T., Convective Heat Transfer Coefficient of some Fruits under Open Sun Drying Conditions, *Journal of Food Technology, 3* (2005), 1, pp. 10-14
[7] Akpinar, E. K., Evaluation of Convective Heat Transfer Coefficient of Various Crops in Cyclone Type Dryer, *Energy Conversion Management, 46* (2005), 15-16, pp. 2439-2454
[8] Togrul, I.T., Pehlivan, D., Modeling of thin Layer Drying Kinetics of some Fruits under Open-Air Sun Drying Process, *Journal of Food Processing Engineering, 65* (2004), 3, pp. 413-425

[9] Kaya, A., *et al.*, Numerical Modeling of Heat and Mass Transfer during Forced Convection Drying of Rectangular Moist Objects, *International Journal of Heat and Mass Transfer, 49* (2006), 17-18, pp. 3094-3103
[10] Kaya, A., *et al.*, Experimental and Numerical Investigation of Heat and Mass Transfer during Drying of Hayward Kiwi Fruits (*Actinidia Deliciosa Planch*), *Journal of Food Engineering, 88* (2008), 3, pp. 323-330
[11] Chandra Mohan, V. P., Talukdar, P., Three Dimensional Numerical Modeling of Simultaneous Heat and Moisture Transfer in a Moist Object Subjected to Convective Drying, *International Journal of Heat and Mass Transfer, 53* (2010), 21-22, pp. 4638-4650
[12] Taymaz, I., *et al.*, Numerical Investigation of Incompressible Fluid Flow and Heat Transfer Across a Bluff Body in a Channel Flow, *Thermal Science, 19* (2015), 2, pp. 537-547
[13] Hong, S. W., Bergles, A. E., Augmentation of Laminar Flow Heat Transfer in Tubes by Means of Twisted-Tape Inserts, *Journal of Heat Transfer, 98* (1976), 2, pp. 251-256
[14] Ray, S., Date, A. W., Laminar Flow and Heat Transfer through Square Duct with Twisted Tape Insert, *International Journal of Heat Fluid Flow, 22* (2001), 4, pp. 460-472
[15] Gui, X., *et al.*, Analysis on Three-Dimensional Flow and Heat Transfer in a Cross Wavy Primary Surface Recuperator for a Micro-Turbine System, *Thermal Science, 19* (2015), 2, pp. 489-496
[16] Naga Sarada, S., *et al.*, Enhancement of Heat Transfer Using Varying width Twisted Tape Inserts, *International Journal of Engineering Sciences and Technology, 2* (2010), 6, pp.107-118
[17] Ahmed-Zaïd, A., *et al.*, Amelioration of the Solar Air Collector Performance: Application to the Yellow Onion and Herring Drying Process (in French), *Revue des Energies Renouvelables, 4* (2001), pp. 69-78
[18] Youcef-Ali, S., Study and Optimization of the Thermal Performances of the Offset Rectangular Plate Fin Absorber Plates, with Various Glazing, *Renewable Energy, 30* (2005), 2, pp. 271-280
[19] Lanjewar, A., *et al.*, Heat Transfer and Friction in Solar Air Heater Duct with W-Shaped Rib Roughness on Absorber Plate, *Energy, 36* (2011), 7, pp. 4531-4541
[20] Antonio, M. G. L., EasyCFD_G V4.1.0 User's Manual, 2012
[21] Rivier, M. *et al.*, *Drying of Mangoes: Practical Guide*, Edition Quae, CTA, Paris, 2009
[22] Launder, B. E., *et al.*, The Numerical Computer of Turbulent Flows, *Computational Methods Applied in Mechanical Engineering, 3* (1974), 2, pp. 269-289
[23] Djilali, N., *et al.*, Calculation of Convective Heat Transfer in Recirculating Turbulent Flows Using Various Near-Wall Turbulence Models, *Numerical Heat Transfert Part A, 16* (1989), 2, pp. 189-212
[24] Rivier, M., *et al.*, *Drying of Mangoes: Practical Guide* (in French), Editions Quae, CTA, Paris, 2009

Paper submitted: June 15, 2015
Paper revised: January 23, 2016
Paper accepted: January 23, 2016